JOURNAL OF SOLID STATE CHEMISTRY 118, 112–116 (1995)

Crystal Structure and Magnetic Properties of $(Ni_{1-x}Mg_x)_6MnO_8$

Hideki Taguchi,[1] Sou Omori, and Mahiko Nagao

Research Laboratory for Surface Science, Okayama University, Okayama 700, Japan

Hiroyasu Kido

Osaka Municipal Technical Institute, Jyoto-Ku, Osaka 536, Japan

and

Masahiko Shimada

Institute for Advanced Materials, Tohoku University, Sendai 980, Japan

Received August 15, 1994; in revised form January 27, 1995; accepted January 31, 1995

Murdochite-type $(Ni_{1-x}Mg_x)_6MnO_8$ ($0 \le x \le 0.6$) was synthesized at 873 K using the precursor method. The cell constants, the (Ni, Mg)–O distance, and the Mn–O distance linearly increase with increasing x. These increases depend on the difference between the ionic radii of the Ni^{2+} and the Mg^{2+} ions. The results of the magnetic measurement display a step in the $1/\chi$–T curve, which corresponds to the Néel temperature (T_N). This step is caused by the mixture of the antiferromagnetic cluster due to the 90° superexchange interaction (Ni^{2+}, Mg^{2+})–O–(Ni^{2+}, Mg^{2+}) and paramagnetic spins for the (Ni^{2+}, Mg^{2+})–O–Mn^{4+} bond.

INTRODUCTION

Ni_6MnO_8 (or Mg_6MnO_8) has the cubic murdochite-type structure with space group *Fm3m* (1–3). This structure is considered to be derived from the rock-salt structure of NiO (or MgO) by the replacement of one-eighth of the Ni^{2+} (or the Mg^{2+}) ions with Mn^{4+} ions and one-eighth with vacancies. The Mn^{4+} ions and vacancies occupy (1 1 1) alternate lattice layers and are ordered within the layers.

Porta *et al.* synthesized Ni_6MnO_8 at low temperature using the precursor method (1). The cell constant of Ni_6MnO_8 is 8.306 ± 0.003 Å. From the magnetic measurement of Ni_6MnO_8 in the temperature range from 100 to 300 K, they reported that Ni_6MnO_8 is antiferromagnetic and the $1/\chi$-T curve is linear within the temperature range from 168 to 294 K. The following values have been determined: The Curie constant (C) is 1.35, the effective magnetic moment (μ_{eff}) is 3.28 μ_B, and the paramagnetic Curie temperature (T_θ) is −65 K.

Porta and Valigi reported that the cell constant of Mg_6MnO_8 is 8.381 ± 0.002 Å (3). Mg_6MnO_8 has a weak antiferromagnetic interaction with $T_\theta = -20 \pm 5$ K, and μ_{eff} in the paramagnetic region is 3.94 ± 0.08 μ_B. Mg_6MnO_8 is generally synthesized at high temperature (over 1173 K) under a flow of oxygen using a solid-state reaction. The X-ray diffraction pattern shows that the sample fired at high temperature is a mixture of Mg_6MnO_8 and MgO (2, 3). Recently, Taguchi and Nagao synthesized Mg_6MnO_8 from the stoichiometric molar ratio of Mg/Mn by using a sol–gel process (4).

Cimino and Indovina measured the catalytic activity of Mg_6MnO_8 and α-Mn_2O_3 for N_2O decomposition (5). Since the catalytic activity of Mg_6MnO_8 is lower than that of α-Mn_2O_3, the Mn^{3+} ions are more active in N_2O decomposition than the Mn^{4+} ions. Taguchi *et al.* synthesized murdochite-type $(Mg_{6-x}Al_x)MnO_8$, in which both the Mn^{3+} and the Mn^{4+} ions coexist and the ratio of Mn^{3+}/Mn^{4+} changes linearly with x (6). The cell constants of $(Mg_{6-x}Al_x)MnO_8$ monotonically decrease with increasing x, and this decrease depends on the ionic radii of the Mg^{2+} and the Al^{3+} ions. The result of the magnetic measurements suggests that both the low-spin and high-spin states of the Mn^{3+} ions coexist in $(Mg_{6-x}Al_x)MnO_8$. In the present study, murdochite-type $(Ni_{1-x}Mg_x)_6MnO_8$ ($0 \le x \le 0.6$) was synthesized in order to study its crystallographic and magnetic properties.

EXPERIMENTAL

$(Ni_{1-x}Mg_x)_6MnO_8$ was prepared using the precursor method reported by Porta *et al.* (1). The powders (3 g)

[1] To whom correspondence should be addressed.

0022-4596/95 $12.00

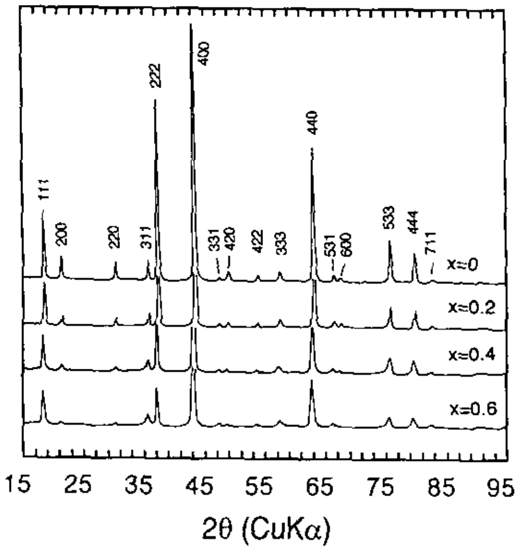

FIG. 1. X-ray powder diffraction patterns for $(Ni_{1-x}Mg_x)_6MnO_8$.

of $Ni(CH_3COOH)_2 \cdot 4H_2O$, $Mg(CH_3COOH)_2 \cdot 4H_2O$, and $Mn(CH_3COOH)_2 \cdot 4H_2O$ were weighed in the desired proportions and dissolved in 100 cm^3 of 0.25 *N* acetic acid. Then, the 0.15 *N* aqueous solution (100 cm^3) of oxalic acid was added. The resulting solution was mixed and evaporated to dryness in a rotary evaporator at 323–343 K. The powder obtained was fired in air at 873 K for 3 hr. The heating rate was 3 K/min.

The phases of the samples were identified by X-ray diffraction (XRD) with monochromatic Cu*K*α radiation. XRD data were collected by step scanning over an angular range $15° \leq 2\theta \leq 95°$ in increments of 0.02° (2θ). The structure refinement was carried out by Rietveld analysis of the X-ray powder diffraction data with the "RIETAN" program written by Izumi (7).

The magnetic susceptibility of the samples was measured by a magnetic torsion balance in the temperature range from 80 to 623 K. Differential scanning calorimetry (DSC) of the sample was performed in the temperature range from 300 to 573 K.

RESULTS AND DISCUSSION

XRD patterns of $(Ni_{1-x}Mg_x)_6MnO_8$ ($0 \leq x \leq 0.6$) were completely indexed as the cubic murdochite-type structure. Figure 1 shows the XRD patterns of $(Ni_{1-x}Mg_x)_6$ $Mn-O_8$. Since the firing temperature was relatively low, the XRD peaks of the samples ($x \geq 0.7$) were broad, so it was difficult to be certain that the sample ($x \geq 0.7$) has a single phase. We carried out the structure refinement of $(Ni_{1-x}Mg_x)_6MnO_8$ ($0 \leq x \leq 0.6$) by Rietveld analysis of XRD data. The space group of Ni_6MnO_8 and Mg_6MnO_8 is *Fm*3*m* (1–3). In the present study, isotropic thermal parameters (*B*) for Ni, Mg, Mn, O(1), and O(2) ions were fixed at 0.2, 0.2, 0.1, 0.1, and 0.3 $Å^2$, respectively. Refined structure parameters and residuals, weighted pattern *R* factor (R_{WP}), pattern *R* factor (R_P), expected *R* factor (R_e), and integrated *R* factor (R_I) are listed in Table 1. The final R_I of all samples was less than 3.06%. The present result suggests that the structure model for $(Ni_{1-x}Mg_x)_6MnO_8$ is good.

Figure 2 shows the relation between the cell constants (*a*-axis) and the composition of *x* in $(Ni_{1-x}Mg_x)_6MnO_8$. The cell constants increase linearly with increasing *x*. The cell constant for Ni_6MnO_8 ($x = 0$) is 8.3200 (2) Å, which is slightly larger than the value reported by Porta *et al.* (1). Since the structure of $(Ni_{1-x}Mg_x)_6MnO_8$ is derived from the rock-salt structure, the coordination number (CN) of the Ni^{2+}, the Mg^{2+}, and the Mn^{4+} ions is 6. The ionic radii of the Ni^{2+} and the Mg^{2+} ions are 0.70 and 0.72 Å, respectively (8). Therefore, the linear increase in the cell constants is explained by the difference between the ionic radii of the Ni^{2+} and the Mg^{2+} ions.

Table 2 shows the (Ni, Mg)–O and the Mn–O distances of $(Ni_{1-x}Mg_x)_6MnO_8$ calculated from the refined structure parameters. In the murdochite-type structure, the (Ni, Mg)–O(1) distance is equal to the Mn–O(1) distance. Both the (Ni, Mg)–O and the Mn–O distances increase with increasing *x*. Figure 3 shows one-eighth of the crystal structure of Ni_6MnO_8. There are two types of NiO_6 octahedrons (A and B). The NiO_6 octahedron (A) has four O(1) and two O(2) ions, and the NiO_6 octahedron (B) has two O(1) and four O(2) ions. In this structure, the NiO_6 octahedra (A) and (B) share edges with each other. The MnO_6 octahedron has two O(1) and four O(2) ions. O(1) ions exist on (0 0 $\frac{1}{4}$) planes, while O(2) ions exist on (0 0 0) and (0 0 $\frac{1}{2}$) planes.

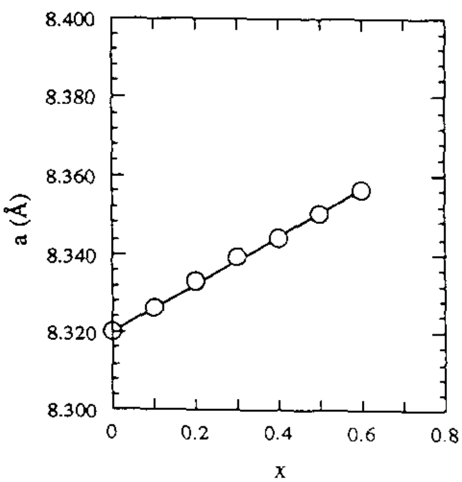

FIG. 2. The cell constants (*a*) vs composition (*x*) for $(Ni_{1-x}Mg_x)_6MnO_8$.

TABLE 1
Refined Structure Parameters for $(Ni_{1-x}Mg_x)_6MnO_8$

$x = 0$ $a = 8.3200(2)$ Å
$R_{WP} = 10.32\%$ $R_P = 7.16\%$ $R_e = 6.33\%$ $R_I = 2.97\%$

Atom	Position	x	y	z	B
Ni	24(*d*)	0	0.25	0.25	0.2
Mn	4(*a*)	0	0	0	0.1
O(1)	8(*c*)	0.25	0.25	0.25	0.1
O(2)	24(*e*)	0.231(2)	0	0	0.3

$x = 0.1$ $a = 8.3226(2)$ Å
$R_{WP} = 9.04\%$ $R_P = 6.45\%$ $R_e = 7.91\%$ $R_I = 2.98\%$

Atom	Position	x	y	z	B
Ni, Mg	24(*d*)	0	0.25	0.25	0.2
Mn	4(*a*)	0	0	0	0.1
O(1)	8(*c*)	0.25	0.25	0.25	0.1
O(2)	24(*e*)	0.231(2)	0	0	0.3

$x = 0.2$ $a = 8.3333(2)$ Å
$R_{WP} = 10.42\%$ $R_P = 7.20\%$ $R_e = 6.47\%$ $R_I = 2.99\%$

Atom	Position	x	y	z	B
Ni, Mg	24(*d*)	0	0.25	0.25	0.2
Mn	4(*a*)	0	0	0	0.1
O(1)	8(*c*)	0.25	0.25	0.25	0.1
O(2)	24(*e*)	0.230(2)	0	0	0.3

$x = 0.3$ $a = 8.3396(2)$ Å
$R_{WP} = 10.11\%$ $R_P = 7.20\%$ $R_e = 6.54\%$ $R_I = 2.58\%$

Atom	Position	x	y	z	B
Ni, Mg	24(*d*)	0	0.25	0.25	0.2
Mn	4(*a*)	0	0	0	0.1
O(1)	8(*c*)	0.25	0.25	0.25	0.1
O(2)	24(*e*)	0.231(2)	0	0	0.3

$x = 0.4$ $a = 8.3442(3)$ Å
$R_{WP} = 10.62\%$ $R_P = 7.94\%$ $R_e = 6.64\%$ $R_I = 2.69\%$

Atom	Position	x	y	z	B
Ni, Mg	24(*d*)	0	0.25	0.25	0.2
Mn	4(*a*)	0	0	0	0.1
O(1)	8(*c*)	0.25	0.25	0.25	0.1
O(2)	24(*e*)	0.231(2)	0	0	0.3

$x = 0.5$ $a = 8.3506(4)$ Å
$R_{WP} = 11.86\%$ $R_P = 8.89\%$ $R_e = 6.76\%$ $R_I = 2.99\%$

Atom	Position	x	y	z	B
Ni, Mg	24(*d*)	0	0.25	0.25	0.2
Mn	4(*a*)	0	0	0	0.1
O(1)	8(*c*)	0.25	0.25	0.25	0.1
O(2)	24(*e*)	0.233(2)	0	0	0.3

$x = 0.6$ $a = 8.3565(4)$ Å
$R_{WP} = 12.58\%$ $R_P = 9.19\%$ $R_e = 6.91\%$ $R_I = 3.06\%$

Atom	Position	x	y	z	B
Ni, Mg	24(*d*)	0	0.25	0.25	0.2
Mn	4(*a*)	0	0	0	0.1
O(1)	8(*c*)	0.25	0.25	0.25	0.1
O(2)	24(*e*)	0.232(2)	0	0	0.3

The magnetic susceptibility (χ) of $(Ni_{1-x}Mg_x)_6MnO_8$ was measured in the temperature range from 80 to 623 K. Figure 4 shows the temperature dependence of the inverse magnetic susceptibility ($1/\chi$). In the range $0 \leq x \leq 0.4$, the $1/\chi$–T curve has a step at 460–480 K for $x = 0$, at 350–380 K for $x = 0.2$, and at 220–250 K for $x = 0.4$. Above the step, each $1/\chi$–T curve obeys the Curie–Weiss law. Although Porta *et al.* reported that Ni_6MnO_8 is antiferromagnetic and obeys the Curie–Weiss law in the temperature range from 168 to 294 K (1), we could not observe the Curie–Weiss law in the $1/\chi$–T curve below the step. As for $x = 0.6$, neither the step nor the Curie–Weiss law has been observed in the temperature range from 80 to 400 K.

The effective magnetic moment (μ_{eff}) was calculated from the high-temperature region where the $1/\chi$–T curve obeys the Curie–Weiss law. Figure 5 shows the relation between the observed μ_{eff} and x. The broken line in Fig. 5 indicates the theoretical μ_{eff} which was calculated on the assumption of the Ni^{2+} ions with the $(d\varepsilon)^6(d\gamma)^2$ and the Mn^{4+} ions with the $(d\varepsilon)^3(d\gamma)^0$. As for $x = 0$ and 0.2, the linear portion obeying the Curie–Weiss law is narrow in comparison with $x = 0.4$ and 0.6. Therefore, the observed μ_{eff} for $x = 0$ and 0.2 deviates from the theoretical μ_{eff}. The decrease in the observed μ_{eff} is caused by the substitution of the Ni^{2+} ions by the Mg^{2+} ions with no 3*d* electrons.

Figure 6 shows the differential scanning calorimetry of Ni_6MnO_8 ($x = 0$) in the temperature range from 300 to 573 K. The unit of heat flow in Fig. 6 is the milliwatt (mW). Ni_6MnO_8 gave a broad exthothermic peak at ca. 475 K. Because Ni_6MnO_8 has the cubic murdochite-type structure at room temperature, it is difficult to bring about the phase transition from cubic to other symmetry at ca.

TABLE 2
(Ni, Mg)–O and Mn–O Distance (Å) for $(Ni_{1-x}Mg_x)_6MnO_8$

x	(Ni, Mg)–O(1)	(Ni, Mg)–O(2)	Mn–O(1)	Mn–O(2)
0	2.080	2.086(1)	2.080	1.918(16)
0.1	2.082	2.087(1)	2.082	1.925(14)
0.2	2.083	2.090(1)	2.083	1.920(16)
0.3	2.085	2.091(1)	2.085	1.925(15)
0.4	2.086	2.092(1)	2.086	1.931(15)
0.5	2.088	2.093(1)	2.088	1.943(17)
0.6	2.089	2.095(1)	2.089	1.940(18)

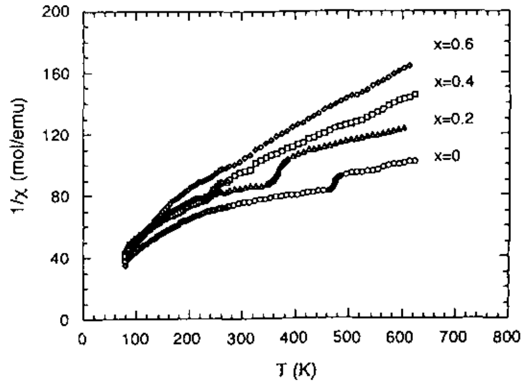

FIG. 4. Inverse magnetic susceptibility ($1/\chi$) vs temperature (T) for $(Ni_{1-x}Mg_x)_6MnO_8$.

475 K. This broad exthothermic peak corresponds to the step in the $1/\chi$–T curve.

Menshikov *et al.* reported that rock-salt type $(Ni_{1-x}Mg_x)O$ ($0.37 < x \leq 0.6$) is antiferromagnetic and has a step in the $1/\chi$–T curve (9). They considered that the step was due to the mixture of the antiferromagnetic cluster and paramagnetic spins. The total magnetic susceptibility, $\chi(T)$, is represented as (9)

$$\chi(T) = \chi_{AF}(T) + \chi_P(T)$$

where $\chi_{AF}(T)$ is the temperature dependence of the antiferromagnetic cluster which displays a common decrease in $\chi(T)$ below T_N, and $\chi_P(T)$ is the Curie–Weiss temperature dependence of the paramagnetic spin susceptibility. In $(Ni_{1-x}Mg_x)_6MnO_8$, the 90° superexchange interactions, (Ni^{2+}, Mg^{2+})–O–(Ni^{2+}, Mg^{2+}) and (Ni^{2+}, Mg^{2+})–O–Mn^{4+}, play an important role with regard to the magnetic properties. It is obvious from Fig. 3 that there is no Mn^{4+}–O–Mn^{4+} bond in $(Ni_{1-x}Mg_x)_6MnO_8$; therefore, we do not need to consider the 90° superexchange interaction (Mn^{4+}–O–Mn^{4+}). NiO exhibits antiferromagnetism with T_N = 520 K and the 90° superexchange interaction (Ni^{2+}–O–Ni^{2+}) is strong and negative (10). From the results of Figs. 4 and 6, the step in the $1/\chi$–T curve of Ni_6MnO_8 is considered to be consistent with T_N. The 90° superexchange interaction (Ni^{2+}–O–Ni^{2+}) is strong and negative, and corresponds to $\chi_{AF}(T)$. On the other hand, the 90° superexchange interaction (Ni^{2+}–O–Mn^{4+}) is weak and positive (11). Thus, the interaction for Ni^{2+}–O–Mn^{4+} is paramagnetic above 80 K and corresponds to $\chi_P(T)$, although the $1/\chi$–T curve does not obey the Curie–Weiss law below the step. With increasing x in $(Ni_{1-x}Mg_x)_6MnO_8$, the Mg^{2+} ions with no $3d$ electrons have increased and the (Ni, Mg)–O and the Mn–O distances have expanded. Consequently, both $\chi_{AF}(T)$ and $\chi_P(T)$ decrease with increasing x. From these results, it is considered that the step in the $1/\chi$–T curve is due to the mixture of the antiferromagnetic cluster ((Ni^{2+},

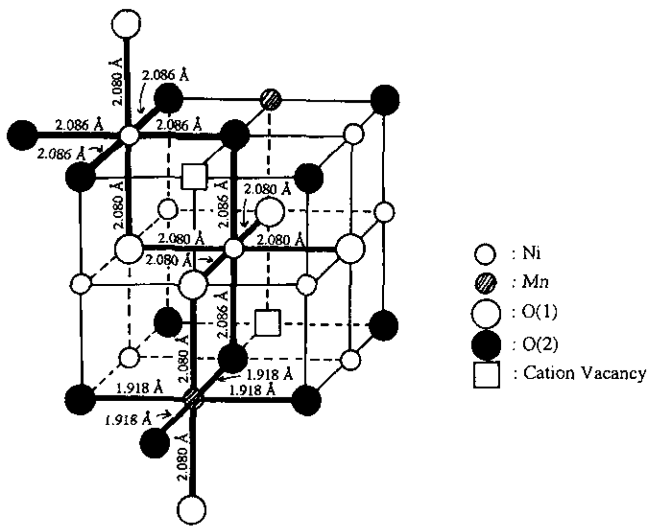

FIG. 3. One-eighth of the crystal structure of Ni_6MnO_8.

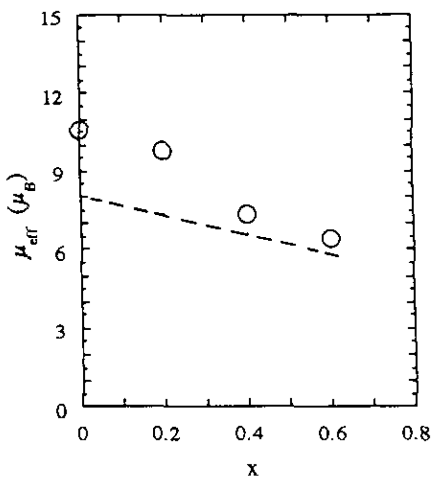

FIG. 5. The effective magnetic moment (μ_{eff}) vs composition (x) for $(Ni_{1-x}Mg_x)_6MnO_8$. Broken line indicates the calculated μ_{eff}.

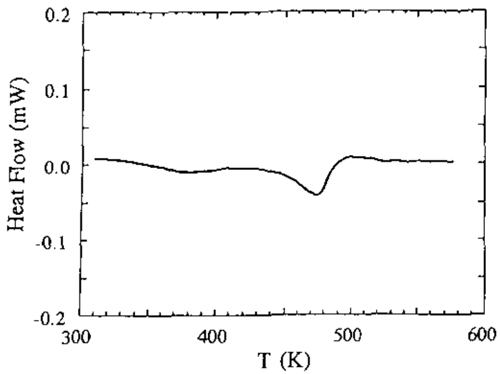

FIG. 6. DSC curve for Ni_6MnO_8.

Mg^{2+})–O–(Ni^{2+}, Mg^{2+})) and paramagnetic spins ((Ni^{2+}, Mg^{2+})–O–Mn^{4+}), and this step shifts to low temperature with increasing x.

CONCLUSION

The structure refinement of $(Ni_{1-x}Mg_x)_6MnO_8$ ($0 \leq x \leq 0.6$) suggests that the cell constants, the (Ni, Mg)–O distance and the Mn–O distance linearly increase with increasing x, and that these increases depend on the difference between the ionic radii of the Ni^{2+} and the Mg^{2+} ions. From the results of the magnetic measurement, the step is observed in the $1/\chi$–T curve, and shifts to low temperature with increasing the number of Mg^{2+} ions. We consider that this step corresponds to T_N and is caused by the mixture of the antiferromagnetic cluster due to the 90° superexchange interaction, (Ni^{2+}, Mg^{2+})–O–(Ni^{2+}, Mg^{2+}), and paramagnetic spins for the (Ni^{2+}, Mg^{2+})–O–Mn^{4+} bond.

REFERENCES

1. P. Porta, G. Minelli, I. L. Botto, and E. J. Baran, *J. Solid State Chem.* **92,** 202 (1991).
2. J. S. Kasper and J. S. Prener, *Acta. Crystallogr.* **7,** 246 (1954).
3. P. Porta and M. Valigi, *J. Solid State Chem.* **6,** 344 (1973).
4. H. Taguchi and M. Nagao, *J. Mater. Sci. Lett.* **10,** 658 (1991).
5. A. Cimino and V. Indovina, *J. Catal.* **17,** 54 (1970).
6. H. Taguchi, A. Okamoto, M. Nagao, and H. Kido, *J. Solid State Chem.* **102,** 570 (1993).
7. F. Izumi, *Nippon Keshou Gakkaishi,* **27,** 23 (1986). [in Japanese]
8. R. D. Shannon and R. D. Prewitt, *Acta Crystallogr. Sect. B* **25,** 925 (1969).
9. A. Z. Menshikov, Y. A. Dorofeev, A. G. Klimenko, and N. A. Mironova, *Phys. Status Solidi B* **164,** 275 (1991).
10. W. L. Roth, *Phys. Rev.* **110,** 1333 (1958).
11. J. B. Goodenough, "Magnetism and the Chemical Bond," p. 190. Wiley, New York, 1963.